

Optical Properties of Biosynthesized Nano-scaled Eu_2O_3 for Red Luminescence Applications

**H. E. A. Mohamed¹⁻², K. Hkiri¹⁻²⁻³, M. Khenfouch¹⁻², S. Dhlamini²⁻⁵,
M. Henini¹⁻²⁻⁴, M. Maaza¹⁻²**

¹ UNESCO-UNISA Africa Chair in Nanosciences-Nanotechnology, College of Graduate Studies, University of South Africa, Muckleneuk ridge, PO Box 392, Pretoria, South Africa

² Nanosciences African Network (NANOAFNET), iThemba LABS-National Research Foundation of South Africa, 1 Old Faure Road, Somerset West, Western Cape 7129, PO Box 722, South Africa

³ Université de Carthage, Faculté des Sciences de Bizerte, LR01ES15, Laboratoire de physique des matériaux : structure et propriétés, 7021 Zarzouna Bizerte. Tunisie

⁴ School of Physics & Astronomy, Nottingham University, Nottingham NG7 2RD, UK

⁵ Department of Physics, CSET, University of South Africa, Johannesburg, 1710, South Africa

*Corresponding author: Hamza@tlabs.ac.za, Maaza@tlabs.ac.za

Abstract

This contribution reports on the optical properties of bio-synthesised Eu_2O_3 nanoparticles bio-engineered for the first time by a green and cost effective method using aqueous fruit extracts of *Hyphaene thebaica* as an effective chelating and capping agent. The morphology, structural and optical properties of the samples annealed at 500° C were confirmed by using high resolution transmission electron microscope (HR-TEM), X-Ray diffraction analysis (XRD), UV-vis spectroscopy and PL spectrometer. The XRD results confirmed the characteristic body centered cubic (bcc) structure of Eu_2O_3 nanoparticles with an average size of 20 nm. HR-TEM revealed square type morphology with an average size of ~ 6 nm. Electron Dispersion Energy dispersive X-ray Spectroscopy (EDS) spectrum confirmed the elemental single phase nature of pure Eu_2O_3 . Furthermore, the FTIR spectroscopy revealed the intrinsic characteristic peaks of Eu–O bond stretching vibrations. UV-vis reflectance proved that Eu_2O_3 absorbs in a wide range of the solar spectrum from VUV-UV region with bandgap of 5.1 eV. The luminescence properties of such cubic were characterized by an intense red emission centered at 614 nm. It was observed that the biosynthesized Eu_2O_3 nanoparticles exhibit an efficient red-luminescence & hence a potential material as red phosphor.

1. Introduction

Rare-earth oxides play a pivotal role in areas related to materials science in general and photonics associated technologies especially [1]. The exceptional optical, catalytic, and magnetic properties of these compounds have attracted researchers community's attention for years. These compounds have a wide range of applications including phosphors and up-conversion materials among others [2]. Such useful photonics applications originate and related to their 4f-electrons inside 4f shell and are highly affected by the composition and structures of the RE compounds, particularly the complexation state and crystal field of the matrix entrapping the RE ions.

Europium(III) oxide (Eu_2O_3), especially, is mainly used as a red or blue phosphor in television sets and fluorescent lamps, as well as an activator for yttrium-based phosphors in flat screen devices. Likewise, it is the component by excellence in the fluorescent glass industry. Europium oxide consists of 3 stable phases; EuO , Eu_2O_3 or Eu_3O_4 . They are all the allotropes of europium oxide with different crystal structures and a variety of magnetic characteristics whereby ferromagnetic for EuO , anti-ferromagnetic for Eu_3O_4 and paramagnetic for Eu_2O_3 were reported [3]. Among them Eu_2O_3 is a special candidate material due to its elevated mechanical, chemical, thermal, optical and dielectric properties. Europium (III) oxide (Eu_2O_3) also known as di-Europium trioxide or Europia [4] is a rare earth stable sesquioxide chemical of the Eu^{3+}

ion with two common crystal structures which are monoclinic B-Type (mS30, space group = C2/m, No.12) and cubic C-Type structure (cI80, space group = Ia-3, No.206) [6] where C-Type structure matches with manganese (III) oxide. Europium oxidizes and reacts with air at 150-180 °C to form Eu₂O₃ [5- 8].

Various physical and chemical processes are reported for the synthesis Eu₂O₃ NPs like sol gel, precipitation, ball milling, hydrothermal, thermal decomposition, pyrolysis, and hydrolysis [9-16]. Despite of being effective, these chemical and physical methods have their own pros and cons. One of the main disadvantages associated with these methods is the less degree of biocompatibility [17] in bio-photonics applications. Therefore, additional processing of nanoparticles are required by coating them with polymers to increase their compatibility. Wet chemistry based processes usually include the use of hazardous chemicals which can generate toxic waste streams [18]. Physical methods on the other hand are expensive and energy intensive [19]. Green resources like plant extracts are becoming popular for the biosynthesis of multifunctional nanoparticles [20-22]. Recently, natural extracts based synthesis of cerium oxide nanoparticles is demonstrated in which plant extracts are used as a natural bio-reductant and chelating agent. Other biological resources like algae, fungi, bacteria can also be used for biosynthesis [23], but their use is discouraged due to biosafety concerns and sophisticated required infrastructure. Therefore, plants are preferred over other biological means as they provides a relatively simpler and easy platform for biosynthesis of nanoparticles. The nanoparticles produced through green synthesis are naturally capped by plant phytochemicals and therefore, reveals enhanced biocompatibility as compared to physically or chemically synthesized ones [17]. Phytosynthesis of nanoparticles using plant extracts is considered more efficient than using microbes [24]. Within this contribution, it is intended to validate the biosynthesis of highly luminescent & biocompatible Eu₂O₃ nano-particles for biophotonics applications. **In this study, the biosynthesis of Eu₂O₃ nanoparticles using plant extracts is investigated. The morphology, structural and optical properties of the prepared samples are reported.**

2. Experiments

2.1 Biosynthesis process of Eu₂O₃ using *Hyphaene thebaica*

Hyphaene thebaica L. Mart is locally known as “Doum” native to Upper Egypt and reported in Egyptian traditional medicines [25]. Pytochemical studies indicated that the fruits contain bioactive compounds such as phenols, flavonoids, alkaloids and vitamins [26]. The fruit part of *Hyphaene thebaica* was collected from Egypt and washed with distilled water to remove any of the particulate matter or derbies, then kept in shade for drying. The dried material was then powdered and used for extraction by introducing 5 g of powdered fruit material into distill water (200 mL) and heated (at 80°C /1 hr) on magnetic stirrer hotplate. The resultant extract solution was cooled to room temperature and filtered three times for the removal of the leftover plant material. The solution was then filtered using Whatman paper n°1, leaving behind transparent aqueous extracts which were used further. The biosynthesis of the Eu₂O₃ NPs was carried out using already established procedure [25]. Briefly 4 g of the precursor salt Ni(II) nitrate hexahydrate (Eu(NO₃)₃. 6H₂O) was added to 100 mL filtered extracts and heated at 80°C/ 1 hrs with gentle stirring, followed by drying in standard oven at 100°C in petri plates. Dried material was scratched and placed in a ceramic boat for annealing in a glass tube furnace in open air at 500°C for 2 hrs. The annealed Eu₂O₃ NPs material were further subjected to intensive physical characterizations.

2.2 Characterizations

Different characterization techniques were used to elucidate the room temperature physical and chemical nature of the nanoparticles. X-ray diffraction pattern (XRD) was obtained at 1.5406 Å Cu K α irradiation line. The pattern was compared with international diffraction database, and crystalline size was calculated using Scherrer approximation. Fourier Transformed Infrared Spectroscopy (FTIR) was performed in spectral range of 400 cm⁻¹ to 4000 cm⁻¹ for finding attached functional responsible for bioreduction and stabilization of nanoparticles. Ultraviolet absorption spectra (UV) of Eu₂O₃ NPs were obtained. Morphology was studied using high Resolution Transmission Electron Microscopy (HR-TEM). HR-TEM images were digitized using Image J software for obtaining size distribution and d-spacing. Energy Dispersive Spectroscopy (EDS) was carried out to determine the elemental composition and Selected Area Electron Diffraction (SAED) pattern was also obtained.

3. Results and discussion

3.1. Structural analysis

To identify, structure, purity and crystallite size, Eu₂O₃ nanoparticles were characterized by X-ray diffraction technique (XRD). Fig. 1 shows the XRD patterns of Eu₂O₃ nanoparticles at room temperature. It can be noted that the diffraction peaks of all samples could be indexed to the Body-centered cubic phase with space group *I* 21 3 which are well matched with the standard JCP2_34-0392. No impurity peaks were observed, indicating the high purity of the final products. Further, the broadness of the XRD peaks specifies the formation of the Nano-sized products. The average crystallite size (D) was estimated from the Debye-Scherer formula; $\langle D \rangle \sim k\lambda / \beta \cos\Theta_B$, where the constant *k* is the shape factor ~ 0.89 , λ is the wavelength of X-ray radiation ($\lambda = 1.5405 \text{ \AA}$) and β is the full width at half maximum of the peak at

diffraction angle Θ_B . The average crystallite size of Eu_2O_3 nanoparticles is found to be around $\langle D \rangle \sim 20$ nm. In order to refine the structural parameters, the XRD pattern of Eu_2O_3 nanoparticles was analyzed by the Rietveld structure refinement method. The structural parameters for the samples were refined so that the calculated pattern fits the observed spectrum very well as shown in Fig. 1 (a). The estimated values of lattices parameters $\langle a \rangle$, $\langle b \rangle$, $\langle c \rangle$ and cell volume $\langle V_{\text{cell}} \rangle$ are found to be $\langle a \rangle = \langle b \rangle = \langle c \rangle \sim 10.8401 \text{ \AA}$, $\langle V_{\text{cell}} \rangle \sim 1273.79 \text{ \AA}^3$, $\langle D \rangle \sim 20.9$ nm. The cell structure of Eu_2O_3 nanoparticles was identified by using the Visualization for Electronic and Structural Analysis (VESTA) program [28], as shown in in Fig. 1(b).

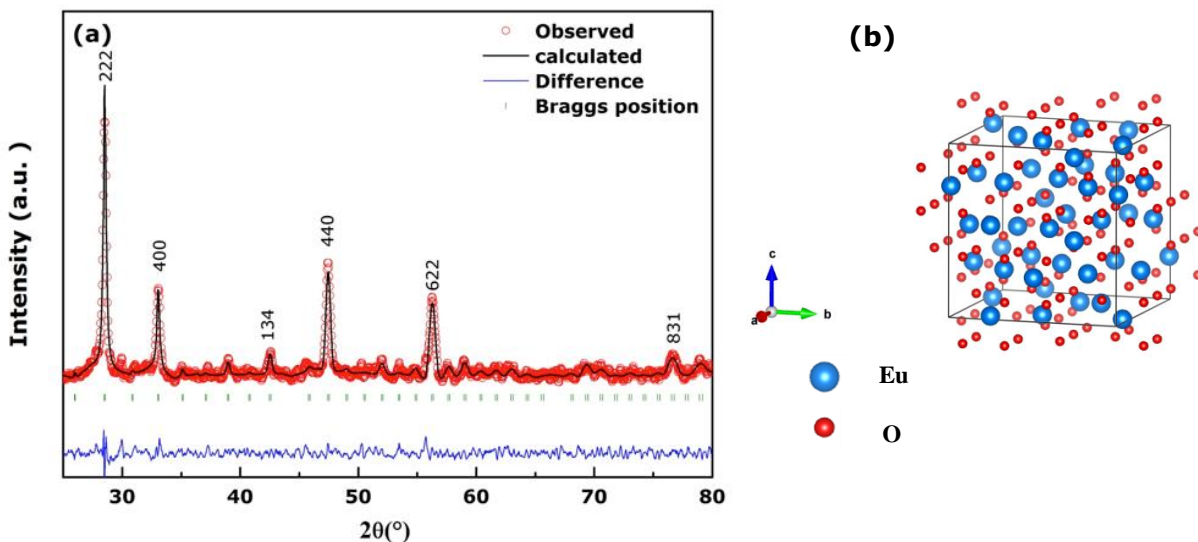
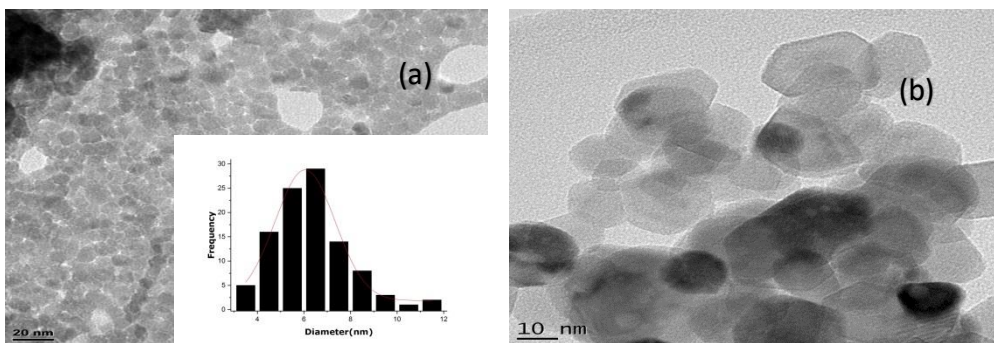


Fig. 1: (a) Rietveld refinement profiles of Eu_2O_3 nanoparticles. The dots are the measured X-ray diffraction data, and the solid line is the calculated profile. The difference curve (observed results minus calculated ones) is plotted at the bottom. The tick marks below represent the positions of Bragg reflections. (b) Crystal structure of the Eu_2O_3 nanoparticles created by VESTA program.

3.2 Morphological and Structural Characteristics



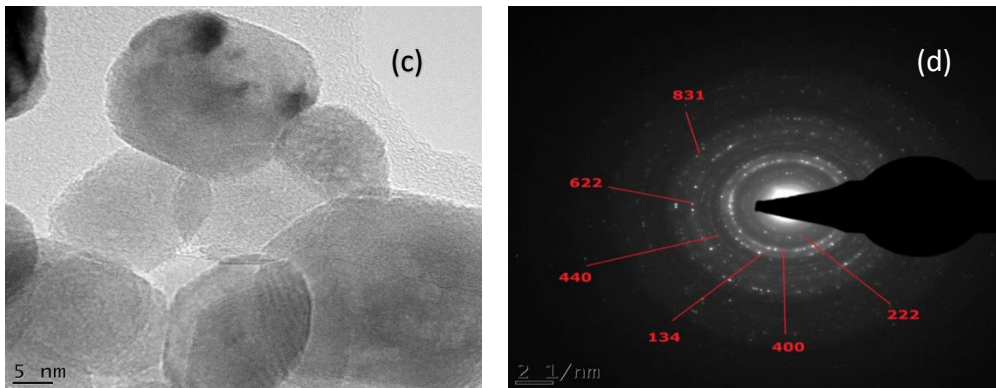


Fig. 2: HR-TEM images (a,b,c) HR-TEM image at different magnifications and their particle size distribution; (d): SAED pattern

Fig 2 shows the various -TEM images of Eu_2O_3 NPs along with the SAED pattern. Different HR-TEM images at different magnifications revealed spherical or quasi-spherical morphology of the particles (Fig a, b, c). These images were processed using image J software and the particle size was obtained that ranges between 2 nm to 12 nm. The average edge length hLi was estimated by fitting the histogram data with a Gaussian distribution peak at ~ 6.1 nm with a standard deviation of 0.21 nm.

The selected area electron diffraction (SAED) analyses were performed in order to investigate the crystallinity of the nanoparticles, from such observations the Eu_2O_3 nanoparticles are polycrystalline with the body centered cubic crystal structure as indicated in Fig 2 d.

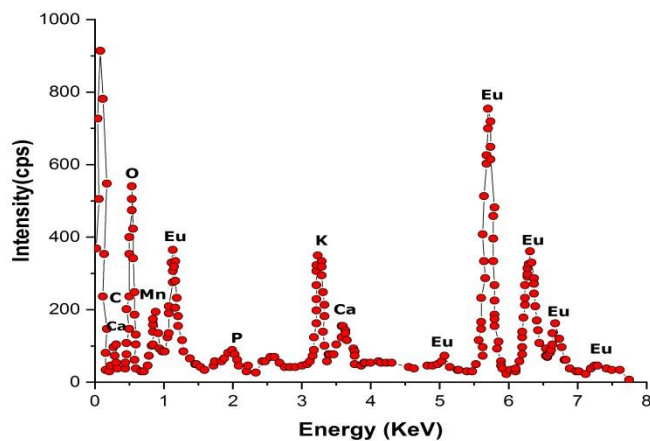


Fig. 3: EDS spectrum of Eu_2O_3 NPs prepared using Hyphaene thebaica.

Fig. 3 reports a typical Energy Dispersive X-Ray Spectroscopy (EDS) spectrum collected with an Oxford instruments X-Max solid state silicon drift detector operating at 20 keV of the annealed Eu_2O_3 NPs at 500°C for 2 h. The obtained spectrum confirmed the presence of Eu, O, C, Ca, Mn, P, Cl, S and K in the annealed powders. The Eu peaks are related to the Eu_2O_3 nanoparticles, O can only be due to Eu_2O_3 nanoparticles and the C originates from the carbon coated grid. The presence of other elements such as Ca, Mn, P, Cl, S and K originates from natural extract as observed in other biosynthesized nano metal oxides. EDS also revealed that at high temperatures, the most abundant elements are Eu and O,

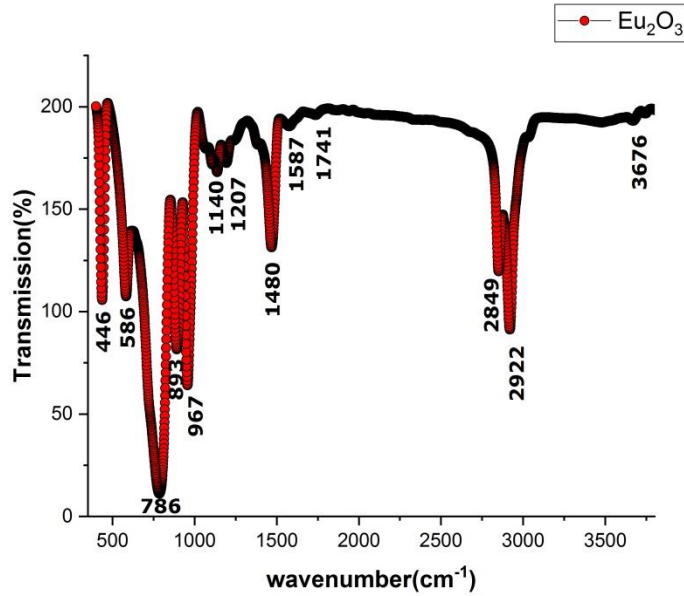


Fig. 4: FT-IR absorption spectra of the Eu_2O_3 NPs annealed at 500°C for 2h.

3.3 FTIR Vibrational properties

Fig. 4 shows the typical FTIR spectrum of the Eu_2O_3 powder in the spectral range of 400 to 4000 cm^{-1} . The FT-IR peaks show all the principal vibrational modes, which are in good agreement with the results reported [29,30]. The FTIR spectra of biosynthesized Eu_2O_3 shows that the characteristic vibration modes are at 446 cm^{-1} , 586 cm^{-1} , 786 cm^{-1} , 893 cm^{-1} , 967 cm^{-1} , 1140 cm^{-1} , 1207 cm^{-1} , 1480 cm^{-1} , 1587 cm^{-1} , 1741 cm^{-1} , 2849 cm^{-1} , 2922 cm^{-1} and 3676 cm^{-1} . The absorption peaks at 446 cm^{-1} and 586 cm^{-1} are attributed to Eu bending showing the Eu_2O_3 NPs formation. The peaks at 786 cm^{-1} and 893 cm^{-1} are attributed to the O-H bending vibration, and the peaks at 1480 cm^{-1} and 1587 cm^{-1} are ascribed to the asymmetric N-O stretching and N-H bending respectively. Peaks at 1140 cm^{-1} and 1207 cm^{-1} correspond to the C-O stretches. The peak at 1741 cm^{-1} corresponds to the C = O. The characteristic stretching frequencies at 2849 cm^{-1} and 2922 cm^{-1} are assigned to C-H stretch band and the absorption broad peak at 3676 cm^{-1} is assigned to OH stretching vibrations of H_2O molecules. Since (Eu) is a heavy metal, its absorbance corresponds to lower frequencies and atoms coordinated to Eu also belong to lower frequencies of vibrations [31].

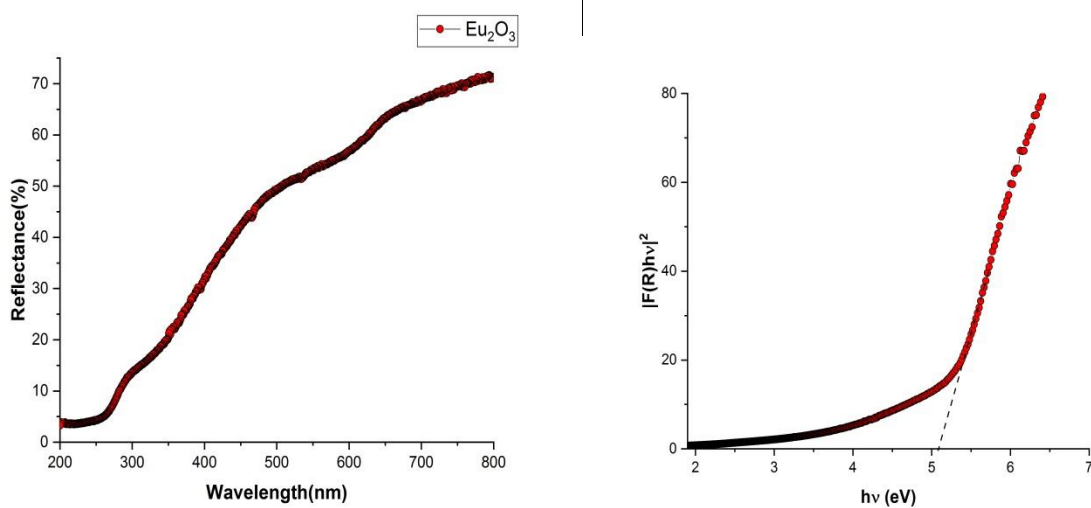


Fig5: (a) Diffuse Reflectance Spectra of Eu_2O_3 NPs, and (b) $[F(R)hv]^2$ versus energy for direct band gap.

3.4 UV-Vis Analysis.

To determine the optical energy gap, Eu_2O_3 NPs we used diffuse reflectance spectroscopy (DRS). Fig. 5 (a) shows the UV-VIS diffused reflectance spectra of Eu_2O_3 in the 200 - 800 nm wavelength range. The UV- VIS diffused reflectance show a major absorption at 241 nm corresponding to band transition of Eu_2O_3 nanoparticles. The optical band gap energy was determined from the reflectance spectrum using Kubelka-Munk formalism by converting the diffuse reflectance spectra into an equivalent transformed function as given by the following equation [32]

$$F(R) = \frac{(1-R)^2}{2R}$$

where $F(R)$ is the Kubelka-Munk function and R is the diffused reflectance of the powder sample. The optical band gap "Eg" was calculated using the following well known Tauc's relation[32]

$$F(R)h\nu = A (h\nu - E_g)^n$$

where A is a constant, $h\nu$ is the energy of the photons (E), E_g is the optical bandgap energy of the material and $n = 2$ for a direct allowed transition. $[F(R)h\nu]^n$ is plotted against photon energy $h\nu$ and extrapolation of the straight-line portion of the curve to the x-axis determines the bandgap E_g . Fig. 5 (b) shows the direct band gap 'Eg' determined by extrapolating the straight portion of the plotted graph to the energy axis, and was found to be equal to 5.1 eV.

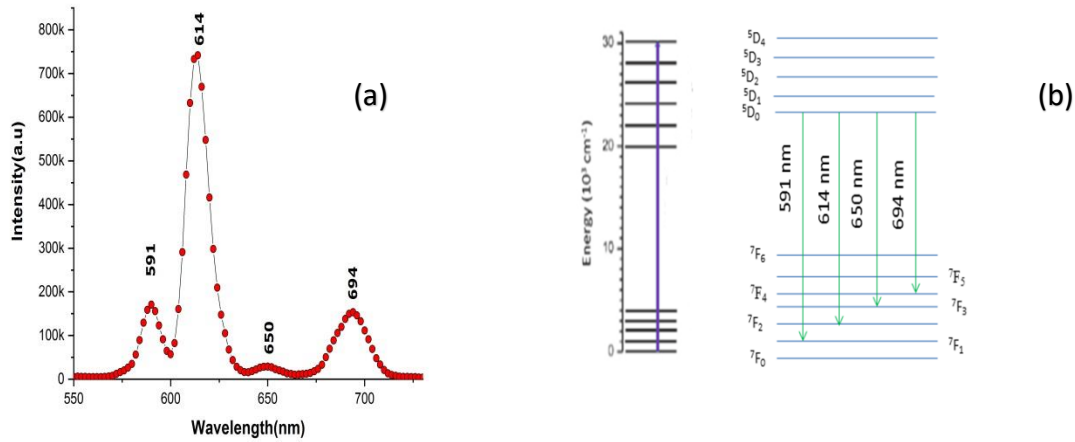


Fig. 6: (a) Room temperature photoluminescence spectra of Eu_2O_3 NPs annealed at 500°C with the excitation wavelength of 254 nm, (b) The energy level diagram of the optical transitions of Eu^{3+} ion and various emission transitions.

3.5 Photoluminescence Properties

Fig. 6 (a) shows the room temperature emission spectra of Eu_2O_3 NPs annealed at 500°C . As can be seen, the Eu_2O_3 nanoparticles exhibit four emission peaks; an orange emission at 591 nm, and three red emissions at 614 nm, 650 nm and 694 nm. Within these emissions, the peak located at 614 nm is the dominant emission since its intensity is the highest. In order to further investigate the obtained photoluminescence spectra, the energy-level diagram of the optical transitions within Eu^{3+} ions is presented in Fig. 6 (b). From this diagram, it is obvious that the emission peak centered at 614 nm is associated with the hypersensitive forced electric dipole transition $^5\text{D}_0 \rightarrow ^7\text{F}_2$. Furthermore, the appearance of this peak confirms the cubic nature of the biosynthesized Eu_2O_3 nanoparticles [27, 33]. The other emission peaks observed located at 591 nm, 650 nm and 694 nm can be attributed to the $^5\text{D}_0 \rightarrow ^7\text{F}_1$, $^5\text{D}_0 \rightarrow ^7\text{F}_3$, and $^5\text{D}_0 \rightarrow ^7\text{F}_4$ optical transitions, respectively. It can be noticed also that as compared to the bulk emission spectra, the photoluminescence spectrum of the biosynthesized Eu_2O_3 nanoparticles exhibits broader bands. Such behavior, which is due to quantum confinement effect associated with the decrease of the particle size, confirms the nanometric aspect of the biosynthesized nanoparticles [27, 31, 34-35].

Conclusion

Green synthesis of nanoparticles provides an ideal platform for synthesizing metal nanoparticles in an economical, safe and easy manner. Using same approach, an extensive study is undertaken to elucidate the physical properties of the Hyphaene thebaica fruit aqueous extract synthesized Eu_2O_3 NPs. The fruit of Hyphaene thebaica is already known for its nutritional and therapeutic importance. Pure and crystalline Eu_2O_3 NPs ~ 20 nm with spherical morphology. The nanoparticles were in the range of 20 nm and different techniques like UV-Vis, EDS, FTIR and TEM confirmed the synthesis of Eu_2O_3 NPs. The PL measurements proved that nano-scaled Eu_2O_3 material exhibit improved fluorescence properties, as the major emission band was centred at about 614 nm due to its well-defined transition within 4d and 4f electron shell which confirm its potential usage in phosphors and luminescence devices. Considering this preliminary encouraging luminescence responses from such a biosynthesized nanoparticle, it is intended to investigate the size effect [36-37] as well as to reproduce such studies on other rare earth oxides in their pure or doped configuration as it was demonstrated previously in the bulk form [38-45].

Acknowledgements

This research was supported by the UNESCO-UNISA Africa Chair in Nanosciences and Nanotechnology (U2ACN2), the National Research Foundation of South Africa (NRF), iThemba LABS, the Abdus Salam International Centre for Theoretical Physics (ICTP), iThemba LABS-NRF, and the Abdus Salam International Centre for Theoretical Physics (ICTP) via the Nanosciences African Network (NANOAFNET) to whom we are all grateful.

Disclosures: The authors declare no conflicts of interest.

References

- [1] P.H. Holloway, T.A. Trottier, B. Abrams, C. Kondoleon, S.L. Jones, 'Advances in field emission displays phosphors', Journal of Vacuum Science & Technology B: Microelectronics and Nanometer, 17-2, 758-764 (1999).
- [2] B.M. Mothudi, O.M. Ntwaeaborwa, J.R. Botha, H.C. Swart, 'Photoluminescence and phosphorescence properties of MAl_2O_4 : Eu^{2+} , Dy^{3+} (M= Ca, Ba, Sr) phosphors prepared at an initiating combustion temperature of 500°C ', Physica B: Condensed Matter 404 (22), 4440-4444 (2009).
- [3] O.M. Ntwaeaborwa, T. Soga, V. Dutta, H.C. Swart, 'Rare earth doped zinc oxide nanophosphor powder: a future material for solid state lighting and solar cells', V Kumar, Acs Photonics 4 (11), 2613-2637 (2017).
- [4] S. Khamlich, B. D. Ngom, C. K. Kotsedi, K. Bouziane, E. Manikandan, M. Maaza, 'Morphological And Crystallographic Properties Of Rare Earth Oxides Coatings Deposited By Double Dual Beam-PLD', Surface Review and Letters (SRL), World Scientific Publishing Co. Pte. Ltd., vol. 21(01), 1-11 (2014).
- [5] S. Ekambaram, M. Maaza, 'Combustion synthesis and luminescent properties of Eu^{3+} -activated cheap red phosphors', Journal of alloys and compounds 395 (1-2), 132-134 (2005).
- [6] S. Ekambaram, K.C. Patil, M. Maaza, 'Synthesis of lamp phosphors: facile combustion approach', Journal of Alloys and Compounds 393 (1-2), 81-92 (2005).
- [7] Y. Li, M. Ge, J. Li, J. Wang, H. Zhang, 'Synthesis of mesoporous Eu_2O_3 microspheres and Eu_2O_3 nanoparticle-wires as well as their optical properties', Society of chemistry, vol. 13, 637-641 (2011).
- [8] S.V Mahajan, D.W Kavich, M.L Redigolo, J.H Dickerson, 'Structural properties of electrophoretically deposited europium oxide nanocrystalline thin films', Journal of material science, vol. 41, 8160-8165 (2006).
- [9] T. Yan, D. Zhang, L. Shi, H. Li. 'Facile synthesis, characterization, formation mechanism and photoluminescence property of Eu_2O_3 nanorods'. Journal of alloys and compounds, 487(1-2):483-488 (2009).
- [10] L. Yang, Y. Tang, and Z. Yang, 'Synthesis of Eu_2O_3 nanowire arrays through a facile sol-gel template approach', J. Sol Gel Sci. Technol. 45, 23-26 (2008).
- [11] D. Zhang, T. Yan, L. Shi, H. Li, J. F. Chiang. 'Template-free synthesis, characterization, growth mechanism and photoluminescence property of $\text{Eu}(\text{oh})_3$ and Eu_2O_3 nanospindles'. Journal of alloys and compounds, 506(1):446-455 (2010).

- [13] J.-M. Li, X.-L. Zeng, Y.-H. Dong, Z.-A. Xu. 'White-light emission and weak antiferromagnetism from cubic rare-earth oxide Eu_2O_3 electrospun nanostructures', *CrystEngComm*, 15(13):2372–2377 (2013).
- [14] A. Panda, G. Glaspell, and M. S. El-Shall, "Microwave synthesis and optical properties of uniform nanorods and nanoplates of rare earth oxides," *J. Phys. Chem. C* 111, 1861–1864 (2006).
- [15] H. Yu, L. Xia, X.-t. Dong, et al. 'Preparation and luminescent characteristics of Eu_2O_3 -zno/(sba-15) composite materials'. *Journal of Luminescence*, 158:19–26 (2015).
- [16] K.-W. Chae, T.-R. Park, C. I. Cheon, N. I. Cho, and J. S. Kim. 'The enhancement of luminescence in co-doped cubic Eu_2O_3 using Li^+ and Al^{3+} ions', *Journal of luminescence*, 131(12):2597–2605, (2011).
- [17] H. E. A. Mohamed, S. Afridi, A. Talha, D. Zia, Z. Khan, M.S.Dhlamini, M. Maaza "Structural , Morphological and Biological Features of ZnO Nanoparticles Using Hyphaene thebaica (L .) Mart . Fruits," *J. Inorg. Organomet. Polym. Mater.*, no. 0123456789, 2020.
- [18] H.E.A. Mohamed, S. Afridi, A.T. Khalil, D. Zia, J. Iqbal, I. Ullah, Z.K. Shinwari, M. Maaza, Biosynthesis of silver nanoparticles from Hyphaene thebaica fruits and their in vitro pharmacognostic potential, *Materials Research Express* (2019).
- [19] H.E.A. Mohamed, S. Afridi, A.T. Khalil, T. Zohra, M.M. Alam, A. Ikram, Z.K. Shinwari, M. Maaza, Phytosynthesis of BiVO_4 nanorods using Hyphaene thebaica for diverse biomedical applications, *AMB Express* 9(1) (2019) 1-14.
- [20] H.E.A. Mohamed, S. Afridi, A.T. Khalil, M. Ali, T. Zohra, R. Akhtar, A. Ikram, Z.K. Shinwari, M. Maaza, Promising antiviral, antimicrobial and therapeutic properties of green nanoceria, *Nanomedicine* (0) (2019).
- [21] A.T. Khalil, I. Khan, K. Ahmad, Y.A. Khan, J. Khan, Z.K. Shinwari, Antibacterial activity of honey in north-west Pakistan against select human pathogens, *J Tradit Chin Med* 34(1) (2014) 86-89.
- [22] M. Ovais, A.T. Khalil, N.U. Islam, I. Ahmad, M. Ayaz, M. Saravanan, Z.K. Shinwari, S. Mukherjee, Role of plant phytochemicals and microbial enzymes in biosynthesis of metallic nanoparticles, *Applied microbiology and biotechnology* 102(16) (2018) 6799-6814.
- [23] F. Thema, E. Manikandan, M. Dhlamini, M. Maaza. 'Green synthesis of zno nanoparticles via agathosma betulina natural extract', *Materials Letters*, 161:124–127 (2015).
- [24] B. Sone, E. Manikandan, A. Gurib-Fakim, and M. Maaza. ' Sm_2O_3 nanoparticles green synthesis via callistemon viminalis' extract', *Journal of Alloys and Compounds*, 650:357–362 (2015).
- [25] N.A. Khalil, A.A. Motaal, A.A. and K. Meselhy, K. Renin and Angiotensin Converting Enzyme Inhibition of Standardized Bioactive Fractions of Hyphaene thebaica L. Mart Growing in Egypt. *Pharmacognosy Journal*, 10(4). (2018).
- [26] M. S. Auwal, I. A. Mairiga, A. Shuaibu, A. Ibrahim, I. A. Gulani, and B. Wampana, "Preliminary phytochemical and in vitro antibacterial evaluation of the crude pericarp extract of Hyphaene thebaica (doumpalm)," *J. Med. Plant Herb. Ther. Res.*, vol. 1, no. 3, pp. 1–7 (2013).
- [27] A. Diallo, B.M. Mothudi, E. manikandan, M. Maaza, 'Luminescent Eu_2O_3 nanocrystals by aspalatus linearis extract: structural and optical properties', *Journal of nanophotonics*, vol. 10(2) (2016).
- [28] K. Momma, F. Izumi. Vesta 3 for three-dimensional visualization of crystal, volumetric and morphology data, *Journal of applied crystallography*, 44(6):1272–1276 (2011).
- [29] S. Chaudhary, A. Umar, 'Glycols functionalized fluorescent Eu_2O_3 nanoparticles effect on the structural and optical properties', *Journal of alloys and compounds*, vol. 682 160-169 (2016).
- [30] J. Kang, Y. Jun, B. Min, Y. Sohn, 'Full characterization of $\text{Eu}(\text{OH})_3$ and Eu_2O_3 nanorods', *Applied surface science* , vol. 314, 158-165 (2014).

- [31] P. Triny Trinh, 'Luminescence studies of europium (III)-D-Glucosamine complexes in water', Department of chemistry, San Jose State University.
- [32] K. Hkiri, H.E.A. Mohamed, M. Ben Salem, A. Kouki, M. Maaza, M. Zouaoui, 'Biosynthesis and characterization of CaZrO₃ nanoparticles via hyphaene thebaica: Effect of preparation method on morphology, electrical and dielectric properties', Journal of Materials Science: Materials in Electronics, vo1 31. 10018–10030 (2020).
- [33] J. Feng, G. Shan, A. Maquieira, M.E. Koivumen, 'Fuctionalized Europium oxide nanoparticles used as fluorescent label in an immunoassay for atrazine', Analytical chemistry, vol. 75, 5282-5286 (2003).
- [34] J. Kang, Y. Jun, B. Min, Y. Sohn, 'Full characterization of Eu(OH)₃ and Eu₂O₃ nanorods', Applied surface science , vol. 314, 158-165 (2014).
- [35] W. Chen, A.G Joly, C.M Kowalchuk, J. Malm, Y. Huang, J Bovin, 'Structure,Luminescence and dynamics of Eu₂O₃ Nanoparticles in MCM-41', Journal of. physics and chemistry, vol. 106, 7034-7041 (2002).
- [36] B.D. Ngom, T. Mpahane, E. Manikandan, M. Maaza, 'ZnO nano-discs by lyophilization process: Size effects on their intrinsic luminescence', Journal of Alloys and Compounds 656, 758-763 (2016).
- [37] S. Chigome, A.A. Abiona, J.A. Ajao, J.B.K. Kana, L. Guerbous, N. Torto, 'Synthesis and Characterization of Electrospun Poly(ethylene oxide)/Europium-Doped Yttrium Orthovanadate (PEO/YVO₄:Eu³⁺) Hybrid Nanofibers', International Journal of Polymeric Materials 59 (11), 863-872 (2010).
- [38] M. Khenfouch, M. Baïtoul, M. Maaza, 'White photoluminescence from a grown ZnO nanorods/graphene hybrid nanostructure', optical Materials 34 (8), 1320-1326 (2012).
- [39] C.M. Magdalane, K. Kaviyarasu, N. Matinise, N. Mayedwa, N. Mongwaketsi, M. Maaza, 'Evaluation on La₂O₃ garlanded ceria heterostructured binary metal oxide nanoplates for UV/visible light induced removal of organic dye from urban wastewater', South African journal of chemical engineering 26, 49-60 (2018).
- [40] A.Y. Fasasi, B.D. Ngom, J.B. Kana-Kana, R. Bucher, M. Maaza, C. Theron, 'Synthesis and characterisation of Gd-doped BaTiO₃ thin films prepared by laser ablation for optoelectronic applications', Journal of Physics and Chemistry of Solids 70 (10), 1322-1329 (2009).
- [41] K Kaviyarasu, P.P. Murmu, J Kennedy, F.T. Thema, D. Letsholathebe, 'Structural, optical and magnetic investigation of Gd implanted CeO₂ nanocrystals', Nuclear Instruments and Methods in Physics Research Section B: Beam,Vol.409,147-152 (2017).
- [42] B. Sathyaseelan, E. Manikandan, K. Sivakumar, J. Kennedy, M. Maaza, 'Enhanced visible photoluminescent and structural properties of ZnO/KIT-6 nanoporous materials for white light emitting diode (w-LED) application',Journal of Alloys and Compounds 651, 479-482 (2015).
- [43] M. Maaza, B.D. Ngom, M. Achouri, K. Manikandan, 'Functional nanostructured oxides', Vacuum 114, 172-187(2015).
- [44] K. Kaviyarasu, C.M Magdalane, E. Manikandan, M. Jayachandran, M. Maaza, 'Well-aligned graphene oxide nanosheets decorated with zinc oxide nanocrystals for high performance photocatalytic application', International Journal of Nanoscience 14 (03), 1550007 (2015).
- [45] S. Khamlich, Z. Abdullaeva, J.V Kennedy, M. Maaza, 'High performance symmetric supercapacitor based on zinc hydroxychloride nanosheets and 3D graphene-nickel foam composite', Applied Surface Science 405, 329-336 (2017).